# EFFECTS OF VISCOSITY AND CONSTRAINTS ON THE DISPERSION AND DISSIPATION OF WAVES IN LARGE BLOOD VESSELS

## II. Comparison of Analysis with Experiments

EVERETT JONES, MAX ANLIKER, *and* I-DEE CHANG

*From the Department of Aeronautics and Astronautics, Stanford University, Stanford, California 94305, and the Ames Research Center of the National Aeronautics and Space Administration, Moffett Field, California 94035*

ABSTRACT The theoretical predictions described in part I of this study are compared with in vivo data from anesthetized dogs. It is shown that the observed attenuation of the pressure and axial waves cannot be accounted for by fluid viscosity alone. For large values of the frequency parameter $\alpha = \sqrt{\rho\omega R_0^2/\mu}$, the analysis of part I is extended to include the effects of viscoelasticity of the vessel wall. The results indicate that the speeds of both types of waves are essentially not affected by a realistic viscoelasticity model while the attenuation per wavelength is significantly increased and becomes frequency independent. The application of this analysis to in vivo data from the carotid arteries of anesthetized dogs demonstrates partial agreement between theory and experiment and suggests that the carotid arteries are anisotropically viscoelastic.

### I. INTRODUCTION

Experimental evidence of the presence of axial and radial waves in fluid-filled, thin-walled latex rubber tubes simulating blood vessels was given by Van Citters (1). Both types of waves were simultaneously generated by a step variation in pressure at one end of the tube. The axial wave had much larger axial wall displacements and a higher speed than the radial wave. Moreover, the axial wave could easily be attenuated by manually gripping the tube. With respect to the wave speeds the observations made by Van Citters have since been partially corroborated in references 2–5.

By utilizing artificially induced pressure signals in the form of finite trains of sine waves (6), it was shown that the aortas of anesthetized dogs are only mildly dispersive for frequences between 40 and 200 Hz. Also, in this frequency range radial waves exhibit strong attenuation and their amplitude portrays an exponential decay

pattern which is independent of frequency when the distance is measured in wavelengths.

The literature to date does not report the natural occurrence of axial waves in arteries and veins. Systematic experimental data on the dispersion and attenuation of induced axial waves have only now become available (7, 8) and suggest an evaluation of the theoretical analysis given in part I.

## II. ELASTIC WALL ANALYSIS

### *Experimental Results from Rubber Tubes*

The experimental results of Van Citters (1) are of particular interest since they corroborate the existence and some of the propagation characteristics of the second type of wave. In these experiments a Penrose tube of 100 cm length was connected to rigid tubing at both ends. The tube was filled with water or glycerin. At one end of the tube a step pressure pulse was produced and near the other end the tube was instrumented to measure pressure and axial and radial wall displacements.

From oscillograph recordings of the disturbances in pressure and wall displacements, Van Citters concluded that two types of waves were generated whose speeds were approximately 6 m/sec and 30 m/sec when the tube was filled with water. The pressure and radial wall displacement appeared to travel at the lowest speed while the axial wall displacement traveled at the faster speed. On the basis of these observations, it was concluded that two independent waves occur: a longitudinal wave with strong axial displacements, and a pressure wave accompanied by large radial wall displacements. Furthermore, it was shown that a manual gripping of the tube, which simulated a distributed external constraint, produces essentially a complete attenuation of the longitudinal waves. Besides this the amplitude of the longitudinal waves was reduced considerably by substituting glycerin for water.

The results of the parametric analysis of part I show that the magnitude of the pressure variation associated with the second type of wave is much smaller than that for the first type of wave. Consequently, the step pressure pulse should excite primarily the first type of wave; however, it can also be demonstrated using part I that the clamps holding the tube onto the rigid tubing will in general require both types of waves to be generated. The exact character of the clamping was not reported and, therefore, the relative strengths of the two types of waves cannot be determined theoretically from the complete solution; but it is apparent from the oscillograph recordings that the pressure fluctuations associated with the second type of wave are much smaller than those for the first type of wave. A comparison of the results in Figs. 6–9 of part I shows that the magnitude of the axial displacements for the second type of wave can still be much larger than those for the first type of wave, even though the magnitudes of the radial wall displacements and pressure fluctuations are extremely small. The parametric analysis of part I also demonstrated that the dissipation of the second type of wave is larger and specifically

predicts a large increase in the dissipation with a weak distributed constraint (the manual gripping). Finally, the ratio of wave speeds $C_2/C_1 \approx 5$ is in agreement with the analytical predictions.

*Experimental Results for Pressure Waves in the Aorta* (6)

Finite trains of small sinusoidal pressure waves were induced in the thoracic aorta of mature mongrel dogs weighing between 20 and 40 kg. These waves were generated by an electrically driven impactor which produced a small indentation of the vessel wall. The pressure signals had amplitudes that were generally less than 5 mm Hg peak-to-peak. Typical results obtained in these experiments for frequencies between 40 and 130 Hz are illustrated in Figs. 1 and 2. From Fig. 1 it follows that the thoracic aorta is only mildly dispersive in respect to pressure waves in this frequency range as predicted by the theoretical results given in part I. The attenuation of such waves in the form of the amplitude ratio $A/A_0$ as a function of the propagation distance measured in wavelengths is shown in Fig. 2. It was found that

$$\frac{A}{A_0} \approx e^{-0.89z/\lambda} \tag{1}$$

independent of frequency. No waves of the second type were observed in these experiments.

The numerical results given in Figs. 2–17 of part I show that for the basic parametric case with elastic walls ($\beta_1 = 10, \beta_2 = 10^2, \sigma = \frac{1}{2}, \Gamma_1 = 0 = \Gamma_2$) the asymptotic or limiting solution for large $\alpha$ is sufficiently accurate for the first type of wave whenever $\alpha > 5$ and for the second type whenever $\alpha > 20$. For most of the larger arteries we have $\alpha > 5$ even at frequencies as low as the normal heart rates.

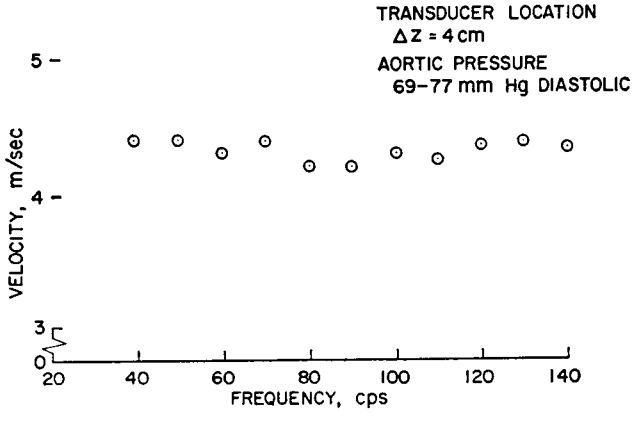


FIGURE 1 Typical dispersion of waves generated in the thoracic aorta of a dog during diastole. Each point represents an average of 3–10 speed measurements of different wave trains at the same pressure levels during diastole (from experiment described in reference 6).

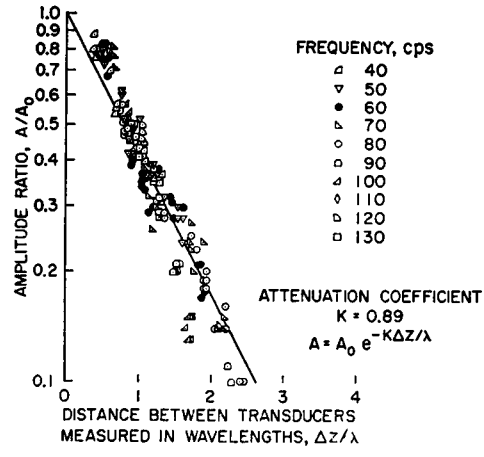


FIGURE 2 Attenuation data for $A/A_0$ plotted on a logarithmic scale. The slope of the line approximating the variation of $\ln(A/A_0)$ with $\Delta z/\lambda$ defines the attenuation coefficient $k$, which in this case is 0.89 (from experiments described in reference 6).

In the case of the thoracic aorta and for frequency between 40 and 130 Hz, $\alpha^2 = \omega R_0^2/\nu$ is a large quantity. Therefore, the experimental results may be compared with the limiting form of the solution for large values of $\alpha$. Measurements of the aorta showed that

$$R_0 \approx 3.83 \text{ mm}, h = 1.35 \text{ mm}.$$

The viscosity coefficient of the blood is assumed to be $\nu = 0.05$ cm$^2$/sec and the vessel wall is considered incompressible, $\sigma = 0.5$. As limiting phase velocity for large frequencies the experiments yield

$$C_0 \approx 4.34 \text{ m/sec}.$$

Since the aorta was surgically exposed in this experiment the vessel is not subjected to distributed constraints and, therefore, $\Gamma_1 = 0 = \Gamma_2$. With these values for $C_0$, $R_0$, and $\nu$ one obtains

$$\beta_2 = \frac{180.5 \text{ Hz}}{f}, \quad \alpha^2 = \frac{f}{0.0544 \text{ Hz}}. \tag{2}$$

From equation 2, $\alpha > 27$ for the frequency range of interest. The limiting form of the solution for large $\alpha$ yields

$$\frac{C_0}{C_1} = \beta_2 \left[\frac{1}{2K_1'}\left(\sqrt{K_3} + \frac{K_2'}{1 - \sigma/2}\right)\right]^{1/2} \left[1 + \frac{K_7}{2\sqrt{2}\alpha}\right], \tag{3}$$

$$\delta_1 \frac{\lambda_1}{R_0} = \frac{\pi K_7}{\sqrt{2}\alpha}, \tag{4}$$

where

$$K_1' = \beta_3\sigma - \frac{A_4}{1 - \sigma/2}, K_2' = \beta_1 + (1 - \Gamma_2)\left(\frac{1}{2} - \frac{1 - \Gamma_1}{2\beta_3}\right), \quad (5)$$

$$K_3 = \left(\frac{K_2'}{1 - \sigma/2}\right)^2 - \frac{4K_1'\beta_1(1 - \Gamma_2)}{\beta_3(1 - \sigma/2)}, C_2' = \beta_1\left(\frac{5}{2} - 2\sigma - \frac{1 - \Gamma_1}{2\beta_3}\right), \quad (6)$$

$$K_4 = 4\left(\frac{K_2'}{1 - \sigma/2}\right)^2\left(\frac{C_2'}{2K_2'} - 1\right) - \frac{4K_1'\beta_1}{\beta_3(1 - \sigma/2)}[\beta_1 - 2(1 - \Gamma_2)], \quad (7)$$

$$K_7 = \left[\frac{C_2'}{1 - \sigma/2} + \frac{K_4}{2\sqrt{K_3}} + 2\sqrt{K_3}\right] \Big/ \left[\sqrt{K_3} + \frac{K_2'}{1 - \sigma/2}\right]. \quad (8)$$

Furthermore, the predicted damping of the sinusoidal waves is given by

$$\frac{A}{A_0} = e^{-\delta_1 z/R_0} = e^{-(\delta_1\lambda_1/R_0)z/\lambda_1} = e^{(-\pi K_7/\sqrt{2}\alpha)\, z/\lambda_1}. \quad (9)$$

This implies that $A/A_0$ is an exponential function proportional to $z/\lambda_1$ ; however, the coefficient of $z/\lambda_1$, the attenuation coefficient $(\delta_1\lambda_1/R_0)$, is not independent of frequency. Also, calculations show that $K_7 \approx 1$ and $\alpha = 27.0$ at 40 Hz, and therefore the attenuation coefficient is only $\pi K_7/\sqrt{2}\alpha = 0.08$ for $f = 40$ Hz and decreases as the frequency increases.

From this result one may conclude that the viscosity of the blood can only account for a small fraction of the attenuation of the sinusoidal pressure waves observed in the thoracic aorta of anesthetized dogs for frequencies between 40 and 130 Hz. Also, since the aorta was exposed, any attenuation of the waves due to the radiation of energy into the surrounding medium may be disregarded. The strong attenuation of the sinusoidal pressure waves must consequently be attributed to damping mechanisms in the aorta wall.

## III. SOLUTION FOR VISCOELASTIC WALL AND LARGE REYNOLDS NUMBERS

To account for the high attenuation of the pressure waves observed in the experiments the vessel wall is now assumed to behave like a viscoelastic solid. Moreover, since the frequencies of the sine waves generated in reference 6 are generally above 20, the corresponding values for $\alpha$ may be considered as large.

Generalizing the approaches of Morgan and Kiely (9) and Chow and Apter (10), one can obtain a solution for the case of a simple viscoelastic wall behavior by simply replacing $E$ and $\sigma$ in equations 3–8 representing the asymptotic solution for large $\alpha$ by

$$E = E_R(\omega) + iE_V(\omega), \sigma = \sigma_R(\omega) + i\sigma_V(\omega). \quad (10)$$

For elastic walls Womersley's analysis (11) produced the result

$$\frac{C_0}{C_1} = X - iY, \tag{11}$$

where the axial and time variation of all quantities is given by the factor

$$e^{i\omega(t-z/C_1)},$$

with $X$ and $Y$ given in tabular form as functions of $\alpha$. Then $C_0/C_1$ contains both wave speed and attenuation factor. Taylor (12) has shown that substitution of $E = E_R + i\omega E_V'$ and $\sigma = \sigma_R + i\omega\sigma_V'$ into Womersley's solution yields

$$\frac{C_{0R}}{C_1} = (X - iY)(1 - i\omega W) \quad \text{where} \quad W = \frac{1}{2}\frac{E_V'}{E_R} + \frac{1}{3}\sigma_V', \tag{12}$$

or, in terms of the parameters used in this analysis,

$$\frac{C_1}{C_{0R}} = \left(\frac{C_1}{C_0}\right)_{\text{elastic}} \Big/ \left[1 - \frac{\omega W}{2\pi}\left(\delta_1\frac{\lambda_1}{R_0}\right)_{\text{elastic}}\right], \tag{13}$$

$$\delta_1\frac{\lambda_1}{R_0} = \left[\left(\delta_1\frac{\lambda_1}{R_0}\right)_{\text{elastic}} + 2\pi\omega W\right] \Big/ \left[1 - \frac{\omega W}{2\pi}\left(\delta_1\frac{\lambda_1}{R_0}\right)_{\text{elastic}}\right]. \tag{14}$$

For large $\alpha$, $[\delta_1(\lambda_1/R_0)]_{\text{elastic}} \ll 1$ and $W \ll 1$, expressions 13 and 14 reduce to

$$\frac{C_1}{C_{0R}} = \left(\frac{C_1}{C_0}\right)_{\text{elastic}} + \text{terms of order } \frac{\omega W}{2\pi}\left(\delta_1\frac{\lambda_1}{R_0}\right)_{\text{elastic}}, \tag{15}$$

$$\delta_1\frac{\lambda_1}{R_0} = \left[\left(\delta_1\frac{\lambda_1}{R_0}\right)_{\text{elastic}} + 2\pi\omega W\right] + \text{terms of order } \omega W\left(\delta_1\frac{\lambda_1}{R_0}\right)_{\text{elastic}} \text{ or } (\omega W)^2\left(\delta_1\frac{\lambda_1}{R_0}\right)_{\text{elastic}}. \tag{16}$$

Utilizing the function $W$ defined in equation 12 McDonald and Gessner (13) have shown that the viscoelastic parameter $\Phi_B$ introduced by Bergel can be related to $W$ by

$$\tan\Phi_B = 2\omega W, \tag{17}$$

where $\Phi_B$ is the viscoelastic parameter presented as experimental data by Bergel.

## IV. VISCOELASTIC DAMPING PARAMETER COMPUTED FROM RECENT DATA (6)

As in the earlier comparison of experimental data with the results of the elastic wall analysis the essential geometric and physical quantities are

$$R_0 = 3.83 \text{ mm}, h = 1.35 \text{ mm}, \beta_1 = 2.8, \sigma_R = \tfrac{1}{2}, \Gamma_1 = 0 = \Gamma_2,$$

$$C_{0R} = 4.34 \text{ m/sec}, \alpha^2 = \frac{f}{0.0544 \text{ Hz}}, \beta_{2R} = \frac{180.5 \text{ Hz}}{f}.$$

Since $\beta_{3R} = 7.5\,\beta_{2R}^2 > 10$ for frequencies less than 150 Hz, the quantity $(1 - \Gamma_1)/\beta_{3R} \ll 1$ even for no distributed radial constraint ($\Gamma_1 = 0$). Making use of this fact in the limiting solution for large $\alpha$, one obtains with equation 10 and with the assumption that $E_V/E_R$ and $\sigma_V$ are small:

$$\frac{C_1}{C_{0R}} = 0.975\left(1 - \frac{0.978}{2\sqrt{2}\alpha}\right), \frac{C_2}{C_{0R}} = 2.84\left(1 - \frac{3.81}{2\sqrt{2}\alpha}\right), \tag{18}$$

$$\delta_1 \frac{\lambda_1}{R_0} = \pi\left[-\left(-\frac{E_V}{E_R} + 0.176\,\sigma_V\right) + \frac{0.978}{\sqrt{2}\alpha}\right], \tag{19}$$

$$\delta_2 \frac{\lambda_2}{R_0} = \pi\left[\left(\frac{E_V}{E_R} + 1.491\,\sigma_V\right) + \frac{3.81}{\sqrt{2}\alpha}\right]. \tag{20}$$

Comparing equation 16 from Taylor's analysis with equation 18 it is apparent that $2\omega W$ and the expression $[(E_V/E_R) - 0.176\,\sigma_V]$ should be equivalent parameters. The relative contribution of the viscous modulus of the wall is the same in $2\omega W$ and $[(E_V/E_R) - 0.176\,\sigma_V]$; however, the contributions of the viscous Poisson's ratio in these viscoelastic parameters differ.

As shown in reference 12, $\delta_i\lambda_i/R_0$ is the logarithmic decrement $k_i$. From the experimental data it follows that $k_1 \approx 0.89 = \delta_1\lambda_1/R_0$. The substitution of this value into equation 19 yields

$$\left(\frac{E_V}{E_R} - 0.176\,\sigma_V\right) = \frac{0.89}{\pi} - \frac{0.978}{\sqrt{2}\alpha} \tag{21}$$

as the pertinent viscoelasticity parameter in the attenuation coefficient. It is plotted in Fig. 3 as a function of frequency together with the experimental data obtained by Anliker et al. (6) and Bergel (14).

According to the data of Bergel, $\Phi_B$ is sufficiently small so that equation 17 can be approximated by

$$2\omega W = \tan \Phi_B \approx \Phi_B.$$

It should be noted that Bergel's results are based on a different viscoelastic model and on measurements conducted in the excised vessels. His viscoelastic attenuation parameter increases with frequency.

For frequencies above 60 Hz, the viscoelastic attenuation parameter as defined by equation 21 is in good agreement with the experimentally measured attenuation coefficient due to all sources of attenuation. From relation 21 it follows that the damp-

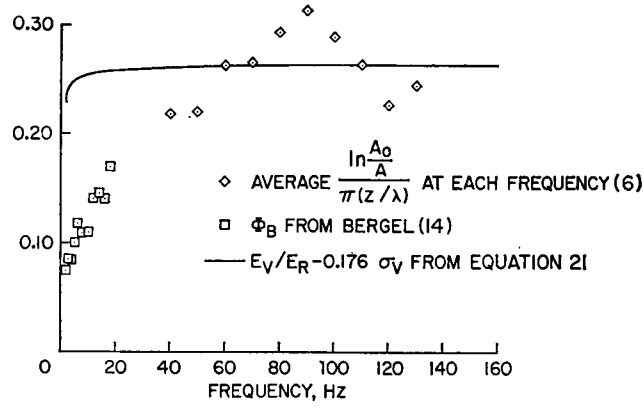


FIGURE 3 A viscoelastic parameter calculated from the data of reference 6.

ing contribution produced by the viscosity of the blood is negligibly small at higher frequencies. Additional data are necessary to determine the individual values of $E_V$, $E_R$, $\sigma_V$, and $\sigma_R$.

## V. COMPARISON OF THEORETICAL ANALYSIS WITH IN VIVO DATA FROM THE CAROTID ARTERY

In the experiments of Anliker et al. (7) and Moritz (8), finite trains of sinusoidal wall displacement waves were induced in the surgically exposed carotid arteries of anesthetized dogs. A plastic collar, which constricted the vessel radius by less than 15%, was displaced sinusoidally along the axis of the artery by an electromagnetic shaker. The frequency range obtained was 25–150 Hz, and the amplitude was usually less than 2 mm peak-to-peak with a maximum amplitude less than 3.5 mm. Local pressure variations were recorded at two locations 3.5–8 cm apart. The axial wall motions at these locations and the pressure records did not reveal any reflected waves.

In the absence of reflected waves, application of equations 40 and 46 in part I at $z = 0$ yields the equations

$$p(0, t) = (P_1 + P_3)e^{i\omega t},$$

$$\zeta(0, t) = \frac{e^{i\omega t}}{\rho\omega^2 R_0}(P_1 M_3 e^{i\phi_3} + P_3 M_4 e^{i\phi_4}),$$

which can be solved for $P_1$ and $P_3$. Their substitution back into equations 40 and 46 of part I leads to

$$p(z, t) = p(0, t)\left[\frac{\rho\omega^2 R_0}{M_4 e^{i\phi_4}}\frac{\zeta(0, t)}{p(0, t)} - 1\right]e^{-i\omega z/C_1}e^{-\delta_1 z/R_0}$$

$$\cdot\left\{1 - e^{i\omega z(1/C_1 - 1/C_2)}e^{(\delta_1 - \delta_2)z/R_0}\left[\frac{M_3}{M_4}e^{i(\phi_3 - \phi_4)} - \frac{\rho\omega^2 R_0}{M_4 e^{i\phi_4}}\frac{\zeta(0, t)}{p(0, t)}\right]\right\}/$$

$$\left[1 - \frac{\rho\omega^2 R_0^2}{M_4 e^{i\phi_4}} \frac{\zeta(0,t)/R_0}{p(0,t)}\right]\Bigg/\left[\frac{M_3}{M_4} e^{(i\phi_3 - \phi_4)} - 1\right],$$

$$\zeta(z,t) = \zeta(0,t)\left[1 - \frac{M_4 e^{i\phi_4}}{\rho\omega^2 R_0^2} \frac{p(0,t)}{\zeta(0,t)/R_0}\right] e^{-i\omega z/C_1} e^{-\delta_1 z/R_0}\left\{\frac{M_3}{M_4} e^{i(\phi_3-\phi_4)}\right.$$

$$+ e^{i\omega z(1/C_1 - 1/C_2)} e^{(\delta_1-\delta_2)\, z/R_0}\left[\frac{M_3}{M_4} e^{i(\phi_3-\phi_4)} \frac{M_4 e^{i\phi_4}}{\rho\omega^2 R_0^2} \frac{p(0,t)}{\zeta(0,t)/R_0} - 1\right]\Bigg/$$

$$\left.\left[1 - \frac{M_4 e^{i\phi_4}}{\rho\omega^2 R_0^2} \frac{p(0,t)}{\zeta(0,t)/R_0}\right]\right\}\Bigg/\left[\frac{M_3}{M_4} e^{i(\phi_3-\phi_4)} - 1\right].$$

$R_0$ for the carotid arteries was approximately 2 mm. The recorded pressure perturbations were of the order of 5 mm of $H_2O$ and the ratio of shaker amplitude/$R_0$ was of the order 1. The artery was also surgically exposed and $\alpha$ for the experimental frequency range was sufficiently large to justify the application of the limiting solution for large $\alpha$.

$$\beta_{2R} M_4 = 3.706\left(1 - \frac{2.773}{\alpha}\right).$$

Consequently, the magnitude of the parameter $(M_4 e^{i\phi_4}/\rho\omega^2 R_0^2)(p(0,\ t)/\zeta(0,\ t)/R_0)$ ranges from $0.1771/\beta_{2R}$ at 25 Hz to $0.0104/\beta_{2R}$ at 90 Hz and, for $\beta_{2R} \geq 10$, it is much smaller than 1.0. Also, from the limiting form of the solution for large $\alpha$, $\beta_{2R} M_3 = 0.2613[1 - (1.469/\alpha)]$ and, therefore $M_3/M_4 \ll 1$. By neglecting all terms involving these two small parameters one obtains

$$p(z,t) = -\frac{\rho\omega^2 R_0}{M_4 e^{i\phi_4}} \zeta(0,t) e^{-i\omega z/C_1} e^{-\delta_1 z/R_0},$$

$$\zeta(z,t) = \zeta(0,t) e^{-i\omega z/C_2} e^{-\delta_2 z/R_0}.$$

These two relations demonstrate that the waves of the first and second type decouple. The pressure wave is dominantly a wave of the first or slow type while the axial wall displacement waves are dominantly waves of the second or fast type. This effect is verified by the recordings shown in Fig. 4 which demonstrate that the transit time for the pressure wave is considerably larger than for the axial displacement wave. The speeds and attenuation for the pressure and axial wall displacement waves as obtained from six experiments are shown in Figs. 5 and 6 together with the corresponding data for torsion waves.

The wall density, fluid density, fluid viscosity, and Poisson's ratio of the wall material were not measured in the experiments and these quantities were assumed to have the values

$$\rho_w = \rho = 1\text{g/cm}^3,\ \nu = 0.05\ \text{cm}^2/\text{sec},\ \sigma_R = \tfrac{1}{2}.$$

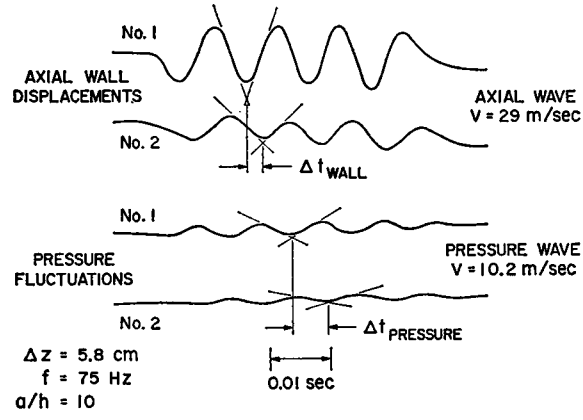


FIGURE 4 Simultaneous recording of pressure and axial wall displacements at two axial locations along the exposed left carotid artery of a dog from reference 7. The finite trains of waves shown were induced by the axial motion of a collar slightly upstream of station No. 1. The wave speeds indicated equal the displacement of the recording stations divided by the accompanying phase shifts. Axial wall displacement waves have significantly larger speeds than pressure waves.

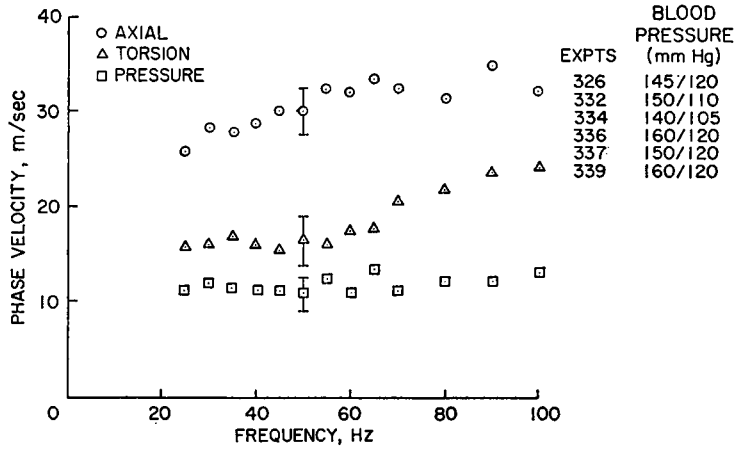


FIGURE 5 Average dispersion pattern of artificially induced axial, torsion, and pressure waves in the exposed carotid artery of six dogs in which all three types of waves were studied. Each data point represents the average of approximately 30 velocity determinations. Also shown are the 95% confidence intervals for each type of wave at 50 Hz. Similar intervals exist at higher and lower frequencies (from reference 8).

The vessel was surgically exposed, hence $\Gamma_1 = 0 = \Gamma_2$. For $R_0 = 2$ mm and $h = 0.25$ mm one obtains $\beta_1 = 8$. With these parameters, large $\alpha$, and large $\beta_{2R}$ the asymptotic solution can be given as

$$\frac{C_{0R}}{C_1} = 1.008\left(1 + \frac{0.379}{\alpha}\right), \frac{C_{0R}}{C_2} = 0.2148\left(1 + \frac{3.15}{\alpha}\right), \qquad (22)$$

$$\delta_1 \frac{\lambda_1}{R_0} = \pi \left[ - \left( - \frac{E_V}{E_R} + 0.06338\, \sigma_V \right) + \frac{1.0706}{\alpha} \right], \tag{23}$$

$$\delta_2 \frac{\lambda_2}{R_0} = \pi \left[ \left( \frac{E_V}{E_R} - 1.397\, \sigma_V \right) + \frac{8.929}{\alpha} \right]. \tag{24}$$

The first and second waves of the analysis were identified with the pressure and axial wall displacement waves respectively of the experiments. This identification was justified previously. From equation 22

$$\frac{C_1}{C_2} = 0.213 \left( 1 + \frac{2.771}{\alpha} \right).$$

According to the data shown in Fig. 5 the ratio of the wave speeds assumes values between 0.40 and 0.43. If we determine the corresponding viscosity parameter from the above equation, we find that $\nu$ would have to range from 0.72 to 2.6 cm²/sec which is entirely unrealistic.

The discrepancy in $C_1/C_2$ between experiment and theory can also not be explained as a result of steady-state or initial loading even though the axial stretch in the carotid arteries was found to be of the order of 40% and the blood pressure was slightly elevated (8); however, there is a strong indication that this discrepancy is a manifestation of anisotropy in the vessel wall behavior. Assuming, for example, that the wall is orthotropic one finds that for the frequency range considered the circumferential modulus of elasticity has a dominant effect on the speed of pressure waves while the axial modulus has a decisive influence on the axial wave speed (15). It appears therefore that the axial Young's modulus is only a fraction of the circum-

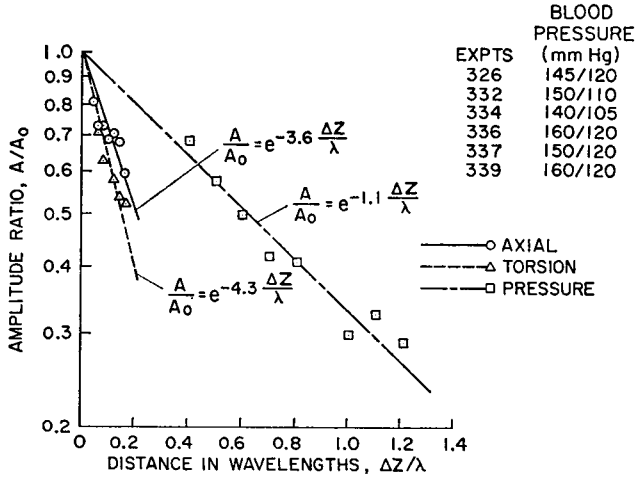


FIGURE 6 Average amplitude ratio from six dogs in which all three types of waves studied were plotted as a function of the distance traveled in wavelengths. (From reference 8).

ferential one. A more detailed investigation of the actual degree of anistoropy is currently in progress.

## VI. CONCLUSIONS

A comparison of the findings of the theoretical study of part I with the experimental results obtained by Van Citters (1) from a mechanical model of a blood vessel showed qualitative and some quantitative agreement. In particular Van Citters's data verify the theoretical prediction that fluid viscosity in the presence of a distributed external constraint can almost completely attenuate the second type of wave. This fact may account for the lack of in vivo evidence of naturally occurring waves of the second type.

The correlation of the theoretical predictions with the data of Anliker et al. (6), however, has indicated that the viscosity of the blood does not produce sufficient dissipation nor does it account for the observed frequency invariance of the attenuation at large $\alpha$. Since experimental information is usually obtained only for large $\alpha$, the solution for this limiting case was modified to include wall viscoelasticity, and the resulting system of equations was used to predict the dissipation of waves of the first type due to the viscoelastic nature of the vessel wall. The data of reference 6 yielded viscoelastic parameters which are of the same order as those found by McDonald and Gessner (13) and as such are much larger than reported otherwise.

This analysis also confirms the decoupling of waves which has been observed experimentally by Anliker et al. (7); however, the predicted ratio of wave speeds does not agree with the experimental data. Wall anisotropy seems to be the cause of the discrepancy.

In addition to the assumption of isotropy and zero initial stresses the solutions given here are subject to two further limitations. First, the restriction to long wavelengths was introduced to simplify the fluid equations and to justify a membrane model for the wall behavior; however, this restriction has so far not been proven an essential contributing factor to a discrepancy between theory and experiment. Second, the linearization of the fluid equations also required the neglecting of the convective acceleration terms. This implies that fluid velocity must at all times be much smaller than the wave speed, but for small $\alpha$ this limitation is no longer tenable.

## NOMENCLATURE

| | |
|---|---|
| $A_4$ | $(\frac{1}{2})(1 - \Gamma_1) - \beta_3[(\frac{1}{2}) - \sigma]$. |
| $C_0$ | Moens-Korteweg wave speed $= \sqrt{Eh/2\rho R_0}$. |
| $C_{0R}$ | Real part of the complex $C_0$. |
| $C_1$ | Wave speed for first type of wave. |
| $C_2$ | Wave speed for second type of wave. |
| $E$ | Modulus of elasticity for the tube wall. |
| $E_R$ | Modulus of elasticity defined by equation 10. |
| $E_V$ | Modulus of elasticity defined by equation 10. |

| | |
|---|---|
| $f$ | Frequency (in Hz). |
| $h$ | Wall thickness. |
| $M_1$–$M_8$ | Mode shape coefficients defined in equations 49–52 of part I. |
| $p$ | Pressure. |
| $P_1$–$P_4$ | Arbitrary constants. |
| $Q$ | Fluid mass flow rate. |
| $r$ | Radial coordinate. |
| $R_0$ | Mean radius of the tube. |
| $t$ | Time. |
| $u$ | Radial velocity component. |
| $w$ | Axial velocity component. |
| $W$ | Function defined in equation 12. |
| $X$, $Y$ | Functions defined by equation 11. |
| $z$ | Axial coordinate. |
| $\beta_{2R}$ | Real part of $\beta_2$. |
| $\alpha$ | $\sqrt{\omega/\nu}R_0$. |
| $\beta_1$ | $(\rho/\rho_w)(R_0/h)$. |
| $\beta_2$ | $C_0/(R_0\omega)$. |
| $\beta_3$ | $2\beta_1\beta_2^2/(1 - \sigma^2)$. |
| $\beta_{3R}$ | Real part of $\beta_3$. |
| $\Gamma_1$ | Radial constraint parameter. |
| $\Gamma_2$ | Axial constraint parameter. |
| $\delta_1$, $\delta_2$ | Dissipation coefficients defined by equation 42 of part I. |
| $\lambda$ | Wavelength. |
| $\lambda_1$ | Wavelength for first type of wave. |
| $\lambda_2$ | Wavelength for second type of wave. |
| $\mu$ | Coefficient of viscosity of fluid. |
| $\nu$ | Kinematic viscosity of fluid. |
| $\rho$ | Fluid density. |
| $\rho_w$ | Wall density. |
| $\sigma$ | Poisson's ratio for the elastic wall. |
| $\sigma_R$, $\sigma_V$ | Defined in equation 10. |
| $\Phi_1$–$\Phi_8$ | Phase angles. |
| $\Phi$ | Angle defined by Bergel and given in equation 17. |
| $\omega$ | Circular frequency. |

This work was carried out at the Ames Research Center of the National Aeronautics and Space Administration under a collaborative research arrangement with Stanford University under National Aeronautics and Space Administration grant NGR 05-020-223.

*Received for publication 26 June 1969 and in revised form 9 October 1970.*

## REFERENCES

1. VAN CITTERS, R. L. 1960. *Circ. Res.* 8:1145.
2. MAXWELL, J. A., and M. ANLIKER. 1966. *In* Biomechanics Symposium. Y. C. Fung, editor. American Society of Mechanical Engineers, New York. 47.
3. MAXWELL, J. A., and M. ANLIKER. 1967. Dispersion and Dissipation of Waves in Blood Vessels. Stanford University SUDAAR Report No. 312, Stanford, Calif.
4. MAXWELL, J. A., and M. ANLIKER. 1968. *Biophys. J.* 8:920.
5. ATABEK, H. B., and H. S. LEW. 1966. *Biophys. J.* 6:481.

6. ANLIKER, M., M. B. HISTAND, and E. OGDEN. 1968. *Circ. Res.* **23**:539.
7. ANLIKER, M., W. E. MORITZ, and E. OGDEN. 1968. *J. Biomech.* **1**:235.
8. MORITZ, W. E. 1969. Transmission characteristics of distension, torsion and axial waves in arteries. Ph.D. Dissertation. Stanford University SUDAAR Report No. 373, Stanford, Calif.
9. MORGAN, G. W., and J. P. KIELY. 1954. *J. Acoust. Soc. Amer.* **25**:323.
10. CHOW, J. D. F., and J. T. APTER. 1968. *J. Acoust. Soc. Amer.* **44**:437.
11. WOMERSLEY, J. R. 1957. An Elastic Tube Theory of Pulse Transmission and Oscillatory Flow in Mammalian Arteries. WADC Technical Report TR 56-614, Wright Air Development Center, Ohio.
12. TAYLOR, M. G. 1959. *Phys. Med. Biol.* **4**:67.
13. MCDONALD, D. A., and U. GESSNER. 1966. Wave Attenuation in Viscoelastic Arteries. Proceedings of First International Conference on Hemorheology. Pergamon Press Ltd., Oxford, England.
14. BERGEL, D. H. 1961. *J. Physiol. (London).* **156**:458.
15. WELLS, M. K. 1969. On the determination of the elastic properties of blood vessels from their wave transmission characteristics. Ph.D. Dissertation. Stanford University SUDAAR Report No. 368, Stanford, Calif.